Optik - International Journal for Light and Electron Optics 182 (2019) 257–268

Contents lists available at ScienceDirect

Optik

journal homepage: www.elsevier.com/locate/ijleo

Original research article

A novel level set approach for image segmentation with landmark constraints

Huizhu Pan*, Wanquan Liu, Ling Li, Guanglu Zhou

School of Electrical Engineering, Mathematical Science and Computing, Curtin University, Perth, WA 6102, Australia

ARTICLE INFO

Keywords:
Image segmentation
Level set method
Landmarks
Chan-Vese model
Split Bregman algorithm

ABSTRACT

Level set methods are widely used in image segmentation and shape analysis. However, most of the current research focuses on fast computational algorithms, initial value selection, and practical applications in various areas. To the best of our knowledge, no research has been conducted on segmentation with level set models where the segmentation contours have to pass through some prior landmark points. In this paper, we propose a new variational model for image segmentation based on the classical Chan-Vese model for this new problem. The new model incorporates prior landmarks information as constraints in a formulated optimization problem. Then, we investigate the theoretical solvability of the new model and design a new algorithm based on the Split Bregman algorithm for numerical implementation. Finally, we conduct some segmentation experiments on gray images and compare with the original Chan-Vese model. The obtained results show many advantages of the proposed model with broad applications. Additionally, we give some critical analysis of the proposed algorithm.

1. Introduction

The goal of image segmentation is to divide an image into different regions according to image features such as edge, intensity, color, texture, motion, and shape, etc. [1]. Image segmentation is an essential part of image analysis and fundamental to many tasks in computer vision, such as object recognition and image interpretation. An abundance of applications of image segmentation can be found in medical image analysis, remote sensing, and surveillance, etc., and appropriate models for segmentation with good performance and their associated efficient algorithms have been popular research topics in the computer vision community.

Variational level set methods have become very influential in image processing and analysis in the past 30 years [2–5]. For segmentation problems, Kass et al. [6] innovatively proposed the ACM (active contour model, or snake model) in 1988 for edge-based image segmentation via energy minimization. Motivated by the ACM, Caselles et al. [7] devised the GAC (geodesic active contours) model based on the minimum weighted length of contours. Meanwhile, in 1989, Mumford and Shah [8] published their famous Mumford–Shah model to approximate the original image with piecewise smooth images and continuous boundaries, establishing a variational framework [9] for region-based image segmentation. The model is described as below

$$\min E(u, \Gamma) = \alpha \int_{\Omega/\Gamma} (u - f)^2 \mathrm{d}x + \beta \int_{\Omega/\Gamma} |\nabla u|^2 \mathrm{d}x + \gamma \int_{\Gamma} \mathrm{d}s \tag{1}$$

where u is a piecewise smooth image, f is the original image, Ω is the image domain, Γ is the continuous boundary, and α, β, and γ are penalty parameters. The first term describes the similarity of the approximated image with the original image, the second term

* Corresponding author.
E-mail address: huizhu.pan@postgrad.curtin.edu.au (H. Pan).

https://doi.org/10.1016/j.ijleo.2019.01.009
Received 22 August 2018; Received in revised form 30 December 2018; Accepted 7 January 2019

describes the smoothness, and the third term represents the minimal length of the contour. It is difficult to solve the Mumford-Shah model directly as shown in (1) because the 2D image and the contour are defined in different spaces. To overcome this problem, Chan and Vese [10] proposed a reduced piecewise constant Mumford-Shah model, i.e., the Chan-Vese model, by combining the variational method and level set method [11] in the variational level set framework [12], which is further explained in Section 2. Based on inheriting advantages such as multi-cue integration from the variational method and adaptive topologies from the level set method, the Chan-Vese model has been successfully extended to the segmentation of different images, including color [13], texture [14], noise [15], intensity [16], and motion [17] images. It has also become the foundation for research in variational multiphase image segmentation [15,16] and, a more recent example, image segmentation using elastica regularized terms for incomplete boundary recovery [18].

Since the Chan-Vese model is highly versatile, much research has been devoted to solving it efficiently. To preserve the level set function as a signed distance function, a computationally intensive re-initialization process is originally involved during the optimization process. In 2005, Li et al. [19] proposed a modified Chan-Vese model without re-initialization via the penalty function method. In 2014, Duan et al. [20] proposed some fast algorithms combining the variable splitting method, dual method, Bregman method, augmented Lagrangian method, and projection method to achieve higher computation efficiency and accuracy without re-initialization.

The Chan-Vese model is a generic model for image segmentation using image region features. It is especially suitable for the segmentation of images with weak boundaries and noise, whereas edge-based models such as the geodesic active contours model [7] can be used for images with more complicated interiors and stronger boundaries. Though many active contour models exist for segmentation, mainly on a case by case basis, the Chan-Vese model has remained significant and widely-used. In this paper, we choose to extend the two-phase region-based Chan-Vese model by introducing landmark points. Explicit information such as feature points has long been used in image analysis, for example, in landmark-based matching in image registration [21]. Inspired by the existing landmark-based image registration models [22–30], we consider a new type of segmentation problem with constraints that induce the contour to pass through some given landmark points. On the other hand, many deep learning methods nowadays are capable of extracting landmark points for segmentation, e.g., FCN for landmark localization [31]. Combining with these automated landmark detection methods, the new proposed model can increase the automation of the segmentation process as well as improve the contour without relying heavily on initialization or parameter tuning. As a practical example, one motivation for using landmarks is that in a problem such as segmentation for eye shape description [32,33], we know that the positions of two eye corners can be detected accurately. Therefore, we need to develop a model for eye shape segmentation with constraints of the eye contours passing through these eye corners. Image-based contour segmentation combined with landmark points, in this case, allows us to retain more biometric information. To the best of our knowledge, no research in facial feature segmentation has undertaken this task.

In this paper, we propose a new model based on the Chan-Vese model by adding landmark constraints to the optimization problem formulation to achieve satisfactory object segmentation. The contour is determined by both image information and the predefined landmarks. Then we investigate the solvability of the proposed model in theory and devise an efficient algorithm for numerical implementation. Experiments show that by introducing landmarks, the new proposed model can improve the accuracy of segmentation significantly as well as correct some faulty regions. Moreover, it can reduce the dependence on contour initialization and penalty parameters tuning which has hindered broader applications of level set models up to now.

This paper is organized as follows. In Section 2, we present the traditional Chan-Vese model in the variational level set framework and introduce its Split Bregman algorithm. In Section 3, we propose the new Chan-Vese model with landmarks constraint (CVL) for image segmentation and provide theoretical justifications. Additionally, we analyze the solvability of the new model and design its Split Bregman algorithm based on the penalty function method. Section 4 presents some experimental results to validate the proposed CVL model and compares its performance with the original Chan-Vese model. Section 5 gives the conclusions.

2. The Chan-Vese model and its Split Bregman algorithm

Before presenting the new model for image segmentation with landmarks, we explain the original Chan-Vese model and one of its numerical solutions in more detail in this section. The Chan-Vese model [10] and Split Bregman algorithm [34] respectively provide the necessary foundation and efficient implementation of our model.

2.1. The Chan-Vese model for image segmentation

In the simplest case, we only consider two-phase image segmentation of gray value images using the variational level set method. For an image $f(x): \Omega \to R$, $x \in \Omega$, assume that the Chan-Vese model divides it into two regions Ω_1, Ω_2 with constant image intensities u_1 and u_2 respectively. In this case, the image can be represented as

$$f(x) = u_1 H(\phi(x)) + u_2(1 - H(\phi(x))) \tag{2}$$

where $\phi(x)$ is a level set function defined as a signed distance function, i.e.,

$$\phi(x) = \begin{cases} d(x, \Gamma) & \text{if } x \in \Omega_1 \\ 0 & \text{if } x \in \Gamma \\ -d(x, \Gamma) & \text{if } x \in \Omega_2, \end{cases} \tag{3}$$

with the property

$$|\nabla\phi(x)| = 1. \tag{4}$$

where Γ represents the contour and (4) denotes the property of a signed distance function and $d(x, \Gamma)$ is the Euclidean distance between x and Γ. $H(\phi(x))$ is the Heaviside function of $\phi(x)$, given by

$$H(\phi(x)) = \begin{cases} 1 & \text{if } \phi \geq 0 \\ 0 & \text{otherwise,} \end{cases} \tag{5}$$

which describes the segmentation contour with a regional change in value. Its partial derivative with $\phi(x)$ is the Dirac function shown below

$$\delta(\phi(x)) = \frac{\partial H(\phi(x))}{\partial \phi(x)}. \tag{6}$$

For easier computation, $H(\phi(x))$ and $\delta(\phi(x))$ are usually changed into a mollified version by introducing a small positive constant parameter ε [10]

$$H_\varepsilon(\phi(x)) = \frac{1}{2}(1 + \frac{2}{\pi}\arctan(\frac{\phi(x)}{\varepsilon})) \tag{7a}$$

$$\delta_\varepsilon(\phi) = \frac{\partial H_\varepsilon(\phi)}{\partial \phi} = \frac{1}{\pi}\frac{\varepsilon}{\phi^2 + \varepsilon^2}. \tag{7b}$$

Now, the Chan-Vese model for image segmentation can be formulated as the following optimization problem,

$$\begin{cases} \min_{u_1,u_2,\phi} E(u_1, u_2, \phi) = \alpha_1 \int_\Omega (f - u_1)^2 H_\varepsilon(\phi)\mathrm{dx} + \alpha_2 \int_\Omega (f - u_2)^2 (1 - H_\varepsilon(\phi))\mathrm{dx} \\ \qquad\qquad + \gamma \int_\Omega |\nabla H_\varepsilon(\phi)|^2 \mathrm{dx} \\ s.\ t. \\ |\nabla\phi| = 1 \end{cases} \tag{8}$$

where α_1, α_2 are penalty parameters for the data terms, γ is a penalty parameter for the length term of the boundary. We can solve for the different components individually. By using the standard variational method and gradient descent method [2], we can obtain the formulas for estimation of u_1 and u_2 as follows

$$u_1 = \frac{\int_\Omega f(x) H_\varepsilon(\phi(x))\mathrm{dx}}{\int_\Omega H_\varepsilon(\phi(x))\mathrm{dx}}, \tag{9a}$$

$$u_2 = \frac{\int_\Omega f(x)(1 - H_\varepsilon(\phi(x)))\mathrm{dx}}{\int_\Omega (1 - H_\varepsilon(\phi(x)))\mathrm{dx}}, \tag{9b}$$

and the evolution equation (segmentation contour) of $\phi(x)$ via gradient descent satisfies the following dynamic equation

$$\begin{cases} \frac{\partial\phi(x,t)}{\partial t} = (\nabla\cdot(\frac{\nabla\phi(x,t)}{|\nabla\phi(x,t)|}) - Q(x, u_1, u_2))\delta_\varepsilon(\phi(x, t)) & t > 0, x \in \Omega \\ \frac{\partial\phi(x,t)}{\partial\vec{n}} = 0 & t > 0, x \in \partial\Omega \\ \phi(x, 0) = \phi^0(x) & t = 0, x \in \Omega \cup \delta\Omega, \end{cases} \tag{10}$$

where $Q(x, u_1, u_2) = \alpha_1(f(x) - u_1)^2 - \alpha_2(f(x) - u_2)^2$.

Until now, we have not considered how to address the constraint $|\nabla\phi(x)| = 1$. Without this constraint, the level set function is not preserved as a signed distance function. Instead of solving this static Hamilton-Jacobi equation, [10] proposed to solve its corresponding dynamic Hamilton-Jacobi equation (10),

We can solve the static Hamilton–Jacobi equation [10] for the constraint via the upwind difference scheme [11], but that process is too complicated. Instead, [10] proposed to solve the following dynamic PDEs based on (10),

$$\begin{cases} \frac{\partial\phi(x,t)}{\partial t} + \sin(\psi(x))(|\nabla\phi(x, t)| - 1) = 0 & t > 0, x \in \Omega \\ \frac{\partial\phi(x,t)}{\partial\vec{n}} = 0 & t > 0, x \in \partial\Omega \\ \phi(x, 0) = \psi(x) & t = 0, x \in \Omega \cup \delta\Omega, \end{cases} \tag{11}$$

via the upwind difference scheme. $\psi(x)$ is the $\phi(x)$ obtained from (10). The new set of equations now maintains the constraint in each iteration. However, the process is still computationally intensive. In particular, solving (10) via the finite difference method [10] involves complicated discretization of curvatures, and solving (11) requires some special upwind schemes for the Hamilton-Jacobi equations. These difficulties have led to many investigations into more efficient algorithms, one of which is the Split Bregman algorithm [34]. On the other hand, as an alternate way to represent the constraint, [19] proposed a penalty function method that incorporates the constraint as a penalty term. Another simple implementation is to use a projection scheme [35,36]. In this paper, we

choose to use the Split Bregman algorithm with the projection method as presented below.

2.2. The Split Bregman algorithm for the Chan-Vese model

To address the computational problems in the Chan-Vese model, Duan et al. [20] designed some fast algorithms using the alternating direction minimization techniques by introducing auxiliary variables and a projection scheme. One of them is the Split Bregman projection method by combining the Split Bregman algorithm and the projection method. The original Split Bregman algorithm was proposed by Goldstein and Osher [35] for imaging sciences. It is, in fact, equivalent to the ADMM (Alternating Direction Method of Multipliers) method [37] and the ALM (Augmented Lagrangian Method) [34]. The projection method is used to overcome the complex computation of Eikonal equations in (8). The Split Bregman projection method for the Chan-Vese model as presented in [20] can be stated as below

$$\begin{cases} (u_1^{k+1}, u_2^{k+1}, \phi^{k+1}, \vec{w}^{k+1}) = \\ \text{argmin}_{u_1,u_2,\phi,w:|\vec{w}|=1} \begin{cases} E(u_1, u_2, \phi, \vec{w}) = & \alpha_1 \int_\Omega (f-u_1)^2 H_\varepsilon(\phi)\mathrm{dx} \\ & +\alpha_2 \int_\Omega (f-u_2)^2 (1-H_\varepsilon(\phi))\mathrm{dx} \\ & +\gamma \int_\Omega |\vec{w}|\delta_\varepsilon(\phi)\mathrm{dx} + \frac{\theta}{2}\int_\Omega |\vec{w} - \nabla\phi - \vec{b}^k|^2 \mathrm{dx} \end{cases} \\ \vec{b}^{k+1} = \vec{b}^k + \nabla\phi^{k+1} - \vec{w}^{k+1} \\ \vec{b}^0 = 0, \vec{w}^0 = \nabla\phi^0, \end{cases} \tag{12}$$

where, $\vec{w}$ is an auxiliary variable to approximate $\nabla\phi$, and $\vec{b}$ is the Bregman iterative parameter. In each loop of iteration, the minimization problem is decomposed into the following three sub-problems,

$$(u_1^{k+1}, u_2^{k+1}) = \text{argmin}_{u_1,u_2} E(u_1, u_2, \phi^k, \vec{w}^k), \tag{13a}$$

$$\phi^{k+1} = \text{argmin}_\phi E(u_1^{k+1}, u_2^{k+1}, \phi, \vec{w}^k), \tag{13b}$$

$$\vec{w}^{k+1} = \text{argmin}_{\vec{w}:|\vec{w}|=1} E(u_1^{k+1}, u_2^{k+1}, \phi^{k+1}, \vec{w}), \tag{13c}$$

By using the standard variational method [2], their solutions can be obtained respectively as

$$u_1^{k+1} = \frac{\int_\Omega f H_\varepsilon(\phi^k(x))\mathrm{dx}}{\int_\Omega H_\varepsilon(\phi^k(x))\mathrm{dx}}, \tag{14a}$$

$$u_2^{k+1} = \frac{\int_\Omega f(1-H_\varepsilon(\phi^k(x))\mathrm{dx}}{\int_\Omega (1-H_\varepsilon(\phi^k(x))\mathrm{dx}}, \tag{14b}$$

$$\begin{cases} Q(u_2^{k+1}, u_2^{k+1})\delta_\varepsilon(\phi(x)) + \gamma|\vec{w}^k(x)|\frac{\partial\delta_\varepsilon(\phi(x))}{\partial\phi(x)} & x \in \Omega \\ -\theta(\Delta\phi(x) - \nabla\cdot\vec{w}^k(x) + \nabla\cdot\vec{b}^k(x)) = 0 & \\ (\vec{w}^k(x) - \nabla\phi(x) - \vec{b}^k(x))\cdot\vec{n} = 0 & x \in \delta\Omega \\ \phi^{k+1,0}(x) = \phi^k(x) & x \in \Omega \cup \delta\Omega, \end{cases} \tag{15}$$

$$\begin{cases} \vec{w}^{k+1}(x) = \max(|\nabla\phi^{k+1}(x) + \vec{b}^k(x)| - \frac{\gamma}{\theta}\delta_\varepsilon(\phi^{k+1}(x)), 0)\frac{\nabla\phi^{k+1}(x) + \vec{b}^k(x)}{|\nabla\phi^{k+1}(x) + \vec{b}^k(x)|_\varepsilon} \\ \vec{w}^{k+1}(x) = \frac{\vec{w}^{k+1}(x)}{\max(1, |\vec{w}^{k+1}(x)|_\varepsilon)}, \end{cases} \tag{16}$$

where (15) is a typical Euler–Lagrange equation on $\phi(x)$ free of complex curvatures, and (16) is a generalized soft thresholding formula in analytical form along with a projection formula [10], which will circumvent the costly re-initialization otherwise required for the constraint through (10) and (11). With help from the auxiliary variables and the projection method, the computation of the Chan-Vese model is now much more efficient. To solve (15), we record it into its gradient descent equation and use the first-order finite difference method temporally and spatially to obtain the Gauss-Seidel iterative scheme for $\phi_{i,j}^{k+1}$ as follows.

$$\phi_{i,j}^{k+1,s+1} = \frac{\begin{pmatrix} \phi_{i,j}^{k+1,s} - \mathrm{tQ}(u_1^{k+1}, u_2^{k+1})\delta_\varepsilon(\phi_{i,j}^{k+1,s}) \\ - t\gamma|\overrightarrow{w}_{i,j}^{k}|\frac{\partial\delta_\varepsilon(\phi_{i,j}^{k+1,s})}{\partial\phi} + t\theta(\nabla\cdot\overrightarrow{b}_{i,j}^{k} - \nabla\cdot\overrightarrow{w}_{i,j}^{k}) \\ + t\theta(\phi_{i-1,j}^{k+1,s+1} + \phi_{i,j-1}^{k+1,s+1} + \phi_{i+1,j}^{k+1,s} + \phi_{i,j+1}^{k+1,s}) \end{pmatrix}}{(1+4t\theta)}, \quad \phi_{i,j}^{k+1,0} = \phi_{i,j}^{k}, \tag{17}$$

until $\frac{|E^{k+1,s+1} - E^{k+1,s}|}{E^{k+1,s}} \le \zeta$. t is the time step, the spatial step is 1, ζ is the error tolerance for accuracy, and $E^{k+1,s} = E(u_1^{k+1}, u_2^{k+1}, \phi^{k+1,s}, \overrightarrow{w}^k)$.

It is worth noting that the above minimization (12) is a typical local minimization problem, which means the final solution depends on initialization conditions, i.e., $\phi^0(x)$ or the initial level set. Typically, the initial level set is fine-tuned [38] along with the penalty parameters α_1, α_2, γ, each representing the importance of the data terms and length term in the segmentation model. This trial and error approach impedes the model from practical applications. On the other hand, by introducing landmark constraints as proposed in this paper, we can lower the dependence of the segmentation results on initialization and bypass some of the fine-tuning as shown in experiments.

3. The Chan-Vese model with constraints on landmarks

The purpose of using landmarks as guidance is to ensure that the segmentation contour passes through some critical locations, despite initialization conditions. To this end, we need to add a constraint to the original Chan-Vese model. Let the landmark points be $\boldsymbol{x_L} = \{x_1, x_2, \ldots, x_L\}$, we can define a mask function for these points as

$$\eta(x) = \begin{cases} 1 & \text{if } x \in \boldsymbol{x_L} \\ 0 & \text{otherwise.} \end{cases} \tag{18}$$

Because we use the zero level set to describe the contour for image segmentation, to guarantee that the landmark points are on the contour, we need to set

$$\phi(x) = 0, \ \text{if } x \in \boldsymbol{x_L}. \tag{19}$$

In this case, the Chan-Vese model should now contain some new constraints as below,

$$\begin{cases} \min_{u_1,u_2,\phi} E(u_1, u_2, \phi) = \alpha_1 \int_\Omega (f-u_1)^2 H_\varepsilon(\phi)\mathrm{d}x + \alpha_2 \int_\Omega (f-u_2)^2(1-H_\varepsilon(\phi))\mathrm{d}x \\ \qquad\qquad + \gamma \int_\Omega |\nabla H_\varepsilon(\phi)|^2 \mathrm{d}x \\ s.\ t. \\ \phi(x) = 0, \ \text{if } x \in \boldsymbol{x_L} \\ |\nabla\phi| = 1. \end{cases} \tag{20}$$

Mathematically, we can incorporate the landmark constraints by augmenting them into a penalty term and adding it to (20), with a new parameter $\mu > 0$,

$$\begin{cases} \min_{u_1,u_2,\phi} E(u_1, u_2, \phi) = \alpha_1 \int_\Omega (f-u_1)^2 H_\varepsilon(\phi)\mathrm{d}x + \alpha_2 \int_\Omega (f-u_2)^2(1-H_\varepsilon(\phi))\mathrm{d}x \\ \qquad\qquad + \gamma \int_\Omega |\nabla H_\varepsilon(\phi)|^2 \mathrm{d}x + \frac{\mu}{2}\int_\Omega \eta(x)\phi^2 \mathrm{d}x \\ s.\ t. \\ |\nabla\phi| = 1, \end{cases} \tag{21}$$

where $\eta(x)$ is (18).

Next, we briefly show that this new functional optimization problem is equivalent to optimization problem with constraint in (20). For $\mu > 0$, we can suppose that $(u_1(\mu), u_2(\mu), \phi(\mu))$ is the unique solution to the problem (19). As to problem (21), we can use the Split Bregman approach to obtain a sequence to approximate its solution as explained in next section. By Theorem 17.1 [39], every limit point (u_1^*, u_2^*, ϕ^*) of the obtained sequence $\{(u_1(\mu^k), u_2(\mu^k), \phi(\mu^k)), k = 0, 1, 2, \ldots\}$ will be the solution of the problem (20). Therefore, a solution of the problem (20) can be obtained by solving (21) for a large positive number $\mu > 0$.

After placing the landmarks on the contour, the effect then propagates from the landmarks to the rest of the contour. An intuitive understanding of the process is as follows. Since $\phi(x)$ is a signed distance function, the value of $\phi(x)$ at individual points is the distance to the segmentation contour. Therefore, setting $\phi(x)$ to 0 for a landmark point not initially on the contour entails that, relative to the landmark, $\phi(x) > 0$ for points closer to the contour and $\phi(x) < 0$ for points farther away, and this causes a new segment of the contour to stem from the landmarks.

We can show the convergence of the model mathematically by analyzing the evolution equation of $\phi(x, t)$ via gradient descent method,

$$\frac{\partial\phi(x,t)}{\partial t} = (\nabla\cdot(\frac{\nabla\phi(x,t)}{|\nabla\phi(x,t)|}) - Q(x, u_1, u_2))\delta_\varepsilon(\phi(x,t)) - \mu\eta(x)\phi(x,t). \tag{22a}$$

At normal points where $\mu\eta(x)\phi(x, t) = 0$, the evolution equation is

$$\frac{\partial\phi(x,t)}{\partial t} = (\nabla\cdot(\frac{\nabla\phi(x,t)}{|\nabla\phi(x,t)|}) - Q(x,u_1,u_2))\delta_\varepsilon(\phi(x,t)), \tag{22b}$$

which shifts the contour in the same way as in the original Chan-Vese model. At the landmark points, $\mu\eta(x)\phi(x,t) \neq 0$, the following equation will be satisfied

$$\frac{\partial\phi(x,t)}{\partial t} = \nabla\cdot(\frac{\nabla\phi(x,t)}{|\nabla\phi(x,t)|})\delta_\varepsilon(\phi(x,t)) - \mu\eta(x)\phi(x,t). \tag{22c}$$

If $\phi(x,t) > 0$, the penalty term will decrease $\phi(x,t)$, and if $\phi(x,t) < 0$, the penalty term will increase $\phi(x,t)$. At points where $\eta(x) = 0$, a more simplified evolution equation is as follows.

$$\frac{\partial\phi(x,t)}{\partial t} = \nabla\cdot(\frac{\nabla\phi(x,t)}{|\nabla\phi(x,t)|})\delta_\varepsilon(\phi(x,t)). \tag{22d}$$

The above is a typical curve interpolation equation via curvature diffusion of an implicit level set function. Therefore, the additional constraint term does not hinder the convergence analysis in comparison with the original model. So far, we have investigated the theoretical effectiveness and convergence of the new model. In the next section, we show how to solve (21) iteratively.

4. Split Bregman algorithm for the Chan-Vese model with constraint on landmarks

In order to design the Split Bregman algorithm of the new model (21), we first introduce an auxiliary variable $\vec{w}(x) = \nabla\phi(x)$ and the Bregman iterative parameter $\vec{b}(x)$, and then transform (21) into the following formulation of alternating iterative minimization problem.

$$\begin{cases} (u_1^{k+1}, u_2^{k+1}, \phi^{k+1}, \vec{w}^{k+1}) = \\ \quad \text{argmin}_{u_1,u_2,\phi,w:|\vec{w}|=1} \begin{cases} E(u_1,u_2,\phi,\vec{w}) = & \alpha_1\int_\Omega (f-u_1)^2 H_\varepsilon(\phi)\mathrm{dx} \\ & +\alpha_2\int_\Omega (f-u_2)^2(1-H_\varepsilon(\phi))\mathrm{dx} \\ & +\gamma\int_\Omega |\vec{w}|\delta_\varepsilon(\phi)\mathrm{dx} + \frac{\mu}{2}\int_\Omega \eta(x)\phi^2\mathrm{dx} \\ & +\frac{\theta}{2}\int_\Omega |\vec{w} - \nabla\phi - \vec{b}^k|^2\mathrm{dx} \end{cases} \\ \vec{b}^{k+1} = \vec{b}^k + \nabla\phi^{k+1} - \vec{w}^{k+1} \\ \vec{b}^0 = 0, \vec{w}^0 = \nabla\phi^0. \end{cases} \tag{23}$$

In each loop of iteration, we would get three sub-problems of minimization,

$$(u_1^{k+1}, u_2^{k+1}) = \text{argmin}_{u_1,u_2} E(u_1,u_2,\phi^k,\vec{w}^k), \tag{24a}$$

$$\phi^{k+1} = \text{argmin}_\phi E(u_1^{k+1}, u_2^{k+1}, \phi, \vec{w}^k), \tag{24b}$$

$$\vec{w}^{k+1} = \text{argmin}_{\vec{w}:|\vec{w}|=1} E(u_1^{k+1}, u_2^{k+1}, \phi^{k+1}, \vec{w}). \tag{24c}$$

The solutions to (24a), (24c) remain the same as (14), (16) respectively, but the evolution equation of $\phi(x,t)$ derived from (24b) becomes

$$\begin{cases} \frac{\partial\phi}{\partial t} = -Q(u_2^{k+1}, u_2^{k+1})\delta_\varepsilon(\phi) - \gamma|\vec{w}^k(x)|\frac{\partial\delta_\varepsilon(\phi)}{\partial\phi} - \mu\eta(x)\phi & t>0, x\in\Omega \\ \quad + \theta(\Delta\phi - \nabla\cdot\vec{w}^k + \nabla\cdot\vec{b}^k) & \\ (\vec{w}^k - \nabla\phi - \vec{b}^k)\cdot\vec{n} = 0 & t>0, x\in\partial\Omega \\ \phi^{k+1,0} = \phi^k & t>0, x\in\Omega\cup\partial\Omega. \end{cases} \tag{25}$$

The Gauss-Seidel iterative scheme for $\phi_{i,j}^{k+1}$ can be derived as follows.

$$\phi_{i,j}^{k+1,s+1} = \frac{\begin{pmatrix} \phi_{i,j}^{k+1,s} - \mathrm{tQ}(u_1^{k+1}, u_2^{k+1})\delta_\varepsilon(\phi_{i,j}^{k+1,s}) \\ - t\gamma|\vec{w}_{i,j}^k|\frac{\partial\delta_\varepsilon(\phi_{i,j}^{k+1,s})}{\partial\phi} + t\theta(\nabla\cdot\vec{b}_{i,j}^k - \nabla\cdot\vec{w}_{i,j}^k) \\ + t\theta(\phi_{i-1,j}^{k+1,s} + \phi_{i,j-1}^{k+1,s} + \phi_{i+1,j}^{k+1,s} + \phi_{i,j+1}^{k+1,s}) \end{pmatrix}}{(1 + t\mu\eta_{i,j} + 4t\theta)}, \quad \phi_{i,j}^{k+1,0} = \phi_{i,j}^k, \tag{26}$$

until $\frac{|E^{k+1,s+1} - E^{k+1,s}|}{E^{k+1,s}} \le \zeta$. ζ is the error tolerance, t is the time step, the spatial step is 1, and $E^{k+1,s} = E(u_1^{k+1}, u_2^{k+1}, \phi^{k+1,s}, \vec{w}^k)$.

Comparing equations (17) and (26), one can find that the complexity of solving the original segmentation problem and the

proposed problem is the same. Therefore, we can solve the new problem easily. The above Split Bregman algorithm for the modified Chan-Vese model with landmarks (21) is summarized in Algorithm 1.

Algorithm 1. The Split Bregman algorithm for the Chan-Vese model with landmarks.

(1) Initialization
setup penalty parameter α_1, α_2, θ, μ
setup iteration number K and tolerance ζ
setup timestep t
setup $\vec{b}^0 = \vec{0}$
read image f, initialize level set function ϕ^0
calculate $\vec{w}^0 = \nabla\phi^0$

(2) Iterations
for k = 1 to K
calculate u_1^{k+1}, u_2^{k+1} by (14)
calculate ϕ^{k+1} by (26)
calculate $\vec{w}^{k+1}$ by (16)
calculate $\vec{b}^{k+1}$ according to (23)
if $\frac{|E^{k+1} - E^{k+1}|}{E^{k+1}} \leq \zeta$, break
endfor

Compared to the algorithm for the original model, Algorithm 1 differs only in the iterative calculation of ϕ which has no impact on the time of convergence. In practical scenarios, the penalty parameters are set to suit specific tasks. The landmark constraint term can be balanced with the data terms and the length term to achieve optimal effect. To place more precedence on the landmark constraints, we can reduce the penalty parameters α_1, α_2 for the data terms and shorten the time step t for the iterative scheme, which allows for the effect of the constraints to be significant enough as well as to be able to propagate after each iteration. In terms of the effect on segmentation, there exists a trade-off between the importance of the image data and the landmarks. To mitigate this trade-off as well as speed up optimization, we can adjust the importance of individual terms during optimization, such as let the data terms take precedence in the initial stages and make landmarks more prominent later on by updating penalty parameters between iterations when a certain threshold is crossed.

To summarize, we have proposed a new model that relies on both prior landmarks and image data based on the classical Chan-Vese model. The new model lets us solve for contours passing through given points in a computationally efficient way, without affecting the convergence property of the designed algorithm. With explicit information guiding the evolution of contour, the segmentation result now depends less on the choice of initial contour. Furthermore, the contour is more accurate in the regions marked by good landmarks. The experiments below demonstrate these advantages.

5. Experimental results

To show the performance of the new model with landmark constraints, we present some segmentation experiments on gray value two-phase synthetic images, a noisy image, and an ultrasound image. We then compare the results with those obtained from the Chan-Vese model. For the experiments below, all initial contours and landmarks are selected by hand, though they may also be generated automatically in the future. The running environment is PC (Intel (R) Core (TM) i7-7700 CPU @ 3.60 GHz 3.60 GHz; memory: 16.0 GB; code running environment: Matlab R2017a). The strengths and weaknesses of the new model are discussed in the sections below.

In the following experiments, α_1 and α_2 are 1, and t is 0.1 throughout for easy tuning. In both the CV and the CVL, γ and θ are increased in the case of noisy images in order to subdue the data terms, subsequently reducing the effect of the noise in the data terms. To raise the importance of the landmark constraints, both μ and θ are set higher to increase the weight of the landmark term while suppressing the data terms. Finally, the threshold ζ is set so that convergence is reached after the contour becomes stable.

5.1. Advantages of CVL

5.1.1. Less parameter tuning

One advantage of using landmarks is the lowered dependence of the segmentation result on the choice of the initial level set and penalty parameters. Since the CVL model is a local minimization problem, different setups of the initial contour may converge to different energy minima. It is sometimes difficult to select the optimal initialization for the Chan-Vese model without resorting to a trial and error approach based on perceived results. However, with some given landmarks as guidance, bad initialization can now converge to good contours without excessive tuning. This effect is shown in Figs. 1 and 2 . It is also worth noting that with some automated landmark detection methods, using the CVL can make the segmentation pipeline more automatic.

In Fig. 1, the second initial contour failed to evolve to the semi-enclosed region in the scissors with the given parameters. The object was under-segmented as a result. However, using the same parameters with CVL along with one landmark facilitated that detection. In this case, the landmark point significantly reduced the segmentation error caused by bad initial contour selection.

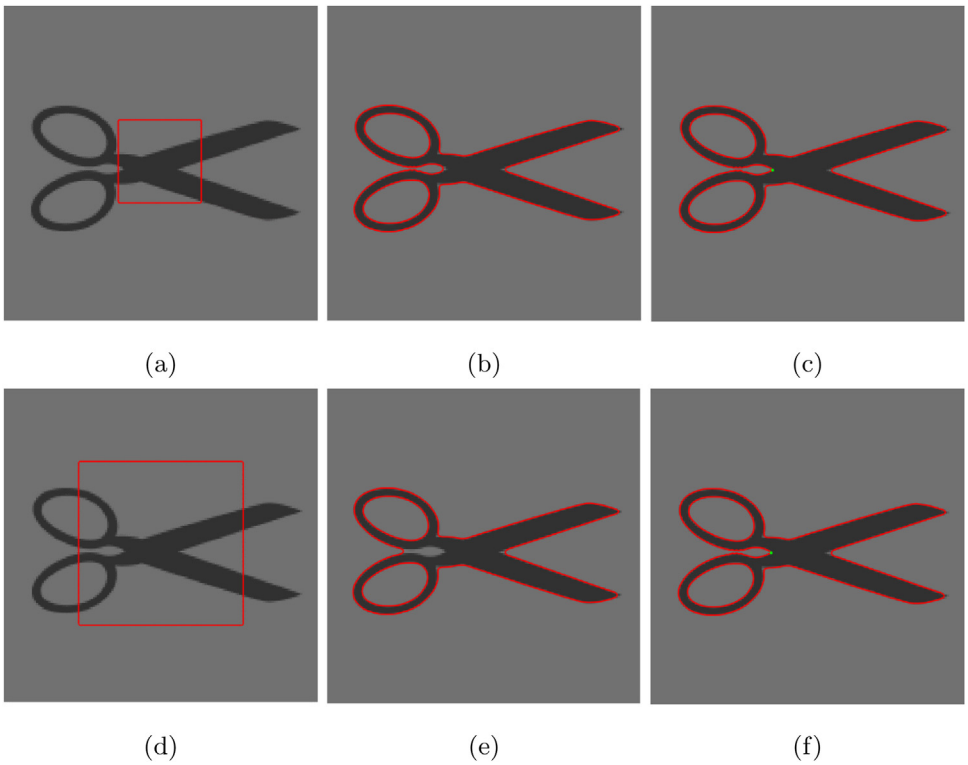

Fig. 1. Synthetic image of scissors. (a-c) and (d-f) use two different initial contours. (c, f) each uses one landmark while (b, e) don't use landmarks. The second initial contour led to under-segmentation, which was fixed by a landmark. In (a-f), $\alpha_1 = 1$, $\alpha_2 = 1$, $\gamma = 1$, $\varepsilon = 3$, $\theta = 20$, $t = .1$, $\zeta = 10^{-6}$. In (c, f), $\mu = 5$.

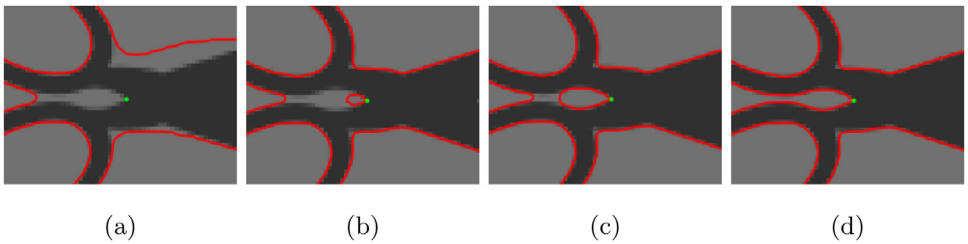

Fig. 2. Synthetic image of scissors, close-up. (a-d) show the evolution of the segmentation contour in the first 25 iterations, in chronological order.

A closer look at the start of the level set evolution shows a section of the contour originating from the landmark in Fig. 2. This is because that numerically the landmark constraint pushed the level set out of an undesirable local energy minimum.

The same correcting effect is demonstrated with a noisy image in Fig. 3. In Fig. 3(c), the segmentation error was due to the choice of parameters rather than the choice of the initial contour. Though a better result may still be generated after parameter tuning, the process would involve more human interference as well as changing other well-segmented parts of the contour through the modified set of parameters. The CVL, on the other hand, completes the task of correction with four landmarks, shown in Fig. 3(d-f). Again, we see that the CVL removed the need for much parameter tuning.

5.1.2. Better contour features

Another advantage of adding landmarks is in improving specific regions of the contour. When certain object features are indistinctly represented in the contour due to image artifacts, poor image quality, or the nature of the segmentation model, we can use landmarks to define and improve them. For instance, we can produce sharper corners in the contour by detecting the corner points and placing them as landmarks, as shown in Figs. 4 and 5 .

In both Figs. 4 and 5, the contours of the objects became more defined with the help of landmarks. When using the original Chan-Vese model, corners are often rounded because of the length minimization term, since minimizing the length of the contour generally entails cutting corners. Instead of resetting the penalty parameters γ and θ, which will influence the segmentation of other regions, we can use the landmark constraint term in CVL to improve the contour description in specific regions. This is useful for segmentation of

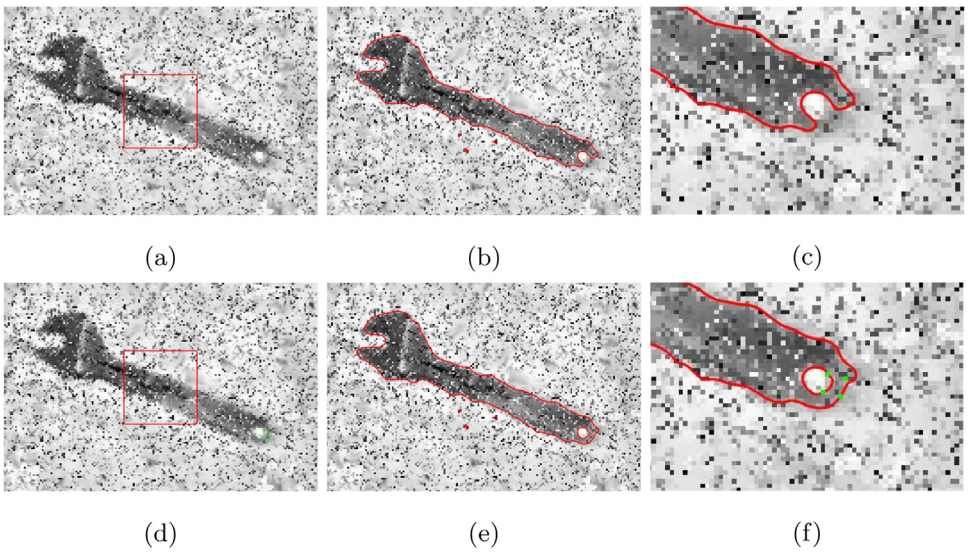

Fig. 3. A wrench with synthetic noise. (a-c) show segmentation without landmarks, (d-f) show segmentation with CVL with four landmarks, and (c, f) are close-ups of the region with complication. In both rows, $\alpha_1 = 1$, $\alpha_2 = 1$, $\gamma = 500$, $\varepsilon = 3$, $\theta = 500$, $t = .1$, $\zeta = 10^{-6}$. In the second row, $\mu = 20$.

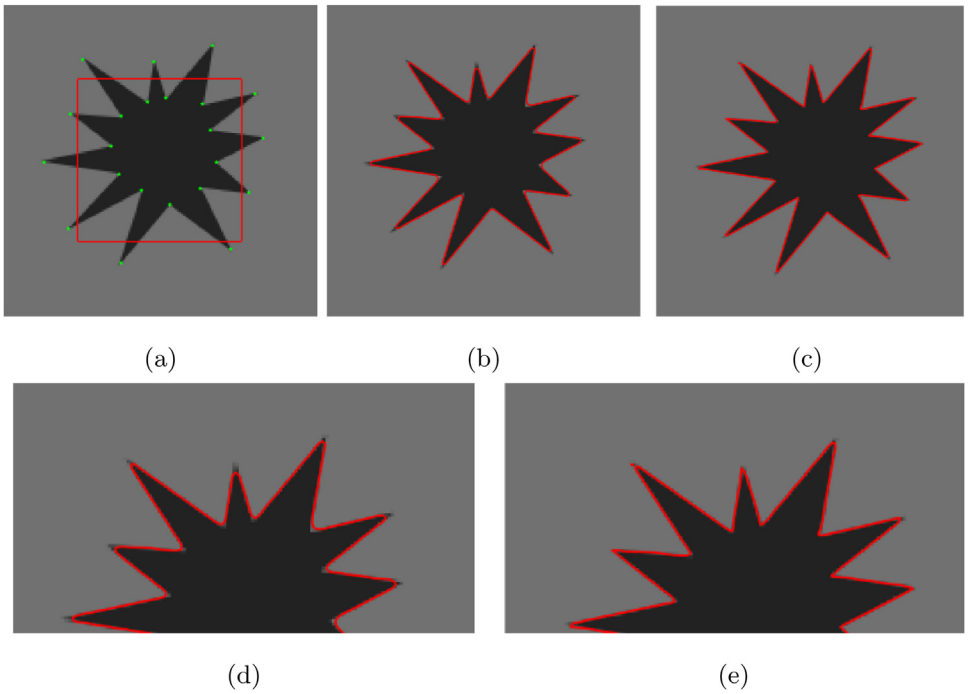

Fig. 4. A star shape. (a) is the original image with initial contour and landmarks, (b) is the segmentation result without landmarks, and (c) is the result using CVL. (d, e) are close-ups of (b, c) respectively. In (a-e), $\alpha_1 = 1$, $\alpha_2 = 1$, $\gamma = 1$, $\varepsilon = 3$, $\theta = 20$, $t = .1$, $\zeta = 10^{-6}$. In (c, e), $\mu = 300$.

critical regions that demand higher accuracy. In particular, establishing the eye corners in eye shape segmentation is likely to improve the description of the eye shapes significantly.

5.2. Analysis on parameter selection of CVL

Sometimes, a landmark is unable to take effect without the importance of the landmark term being raised significantly. As a result, the accuracy of the rest of the contour is negatively affected. An example is shown in Fig. 6.

In Fig. 6, when we segment a triangle with a missing top section using CVL and one landmark, the landmark point initially failed to connect to the contour because it was too far away. Upon increasing the weight of the landmark constraint, the landmark became

Fig. 5. An ultrasound image. (b) is the segmentation result without landmarks, and (c) is the result with CVL and three landmarks. In (b,c), $\alpha_1 = 1$, $\alpha_2 = 1$, $\gamma = 500$, $\varepsilon = 3$, $\theta = 500$, $t = .1$, $\zeta = 10^{-6}$. In (c), $\mu = 500$.

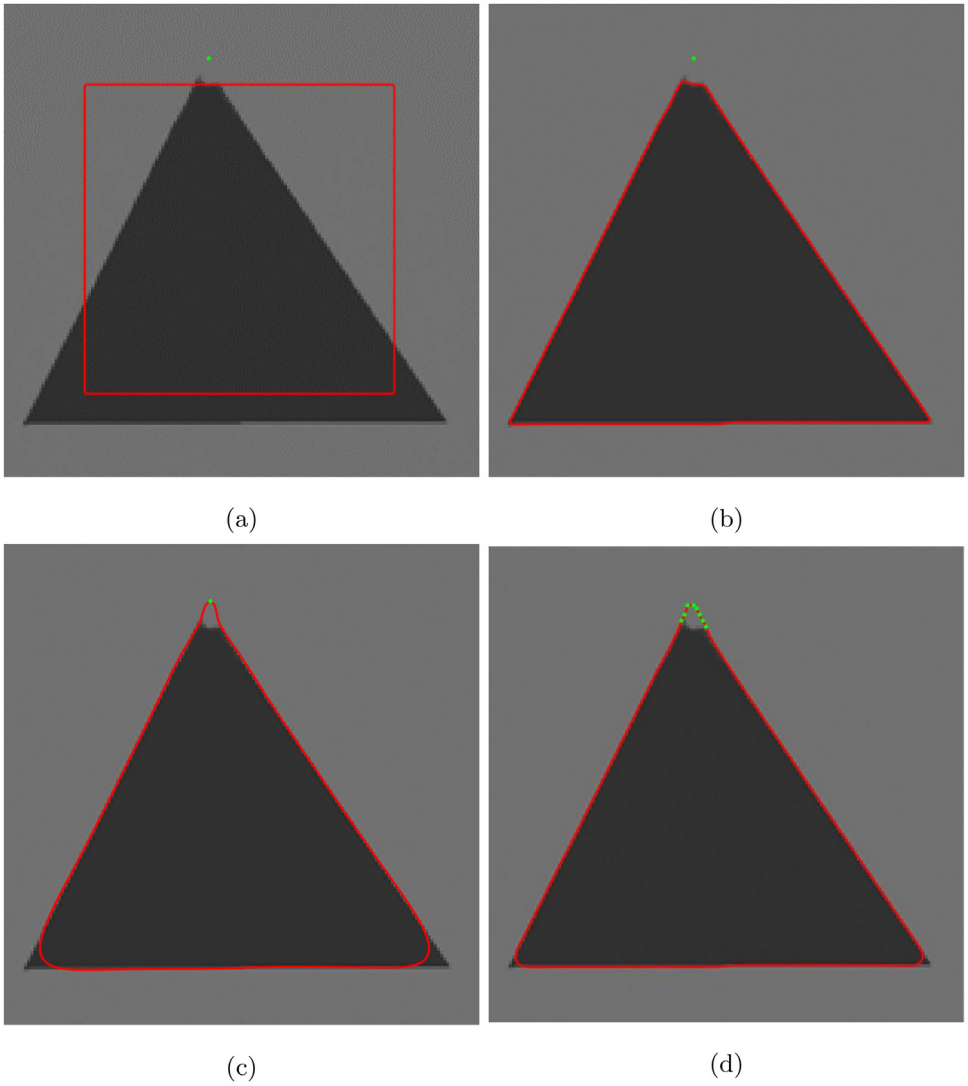

Fig. 6. A damaged triangle. (b) is the segmentation result without using landmarks, (c) is the result using CVL and one landmark, and (d) is the result using CVL with multiple landmarks and more relaxed constraints. In (b-d), $\alpha_1 = 1$, $\alpha_2 = 1$, $\gamma = 1$, $\varepsilon = 3$, $t = .1$. In (b), $\theta = 20$, $\mu = 0$, $\zeta = 10^{-6}$. In (c), $\theta = 5 * 10^5$, $\mu = 5 * 10^5$, $\zeta = 10^{-8}$. In (d), $\theta = 4 * 10^3$, $\mu = 4 * 10^3$, $\zeta = 10^{-6}$.

connected again, albeit that the segmentation result became less accurate due to the data and regularization terms losing their influence. In this case, it appears that forcefully connecting the landmark point through raising the weight of the constraint is impractical. However, when we increased the number of points in Fig. 6 (d), the landmarks worked again, and the need for dramatically increasing the weight of the constraint is circumvented.

Isolated points such as the one in Fig. 6 typically occur when landmarks are placed too far from the object boundary as indicated by image features. They can be detected during the segmentation process when the $\phi(x, t)$ of all points adjacent to these landmark points remain above or below 0 for an extended period, signaling that there was no contour passing through these landmarks for some time. Upon detecting an isolated point, the segmentation process then can be aborted, or, if desired, the point can be removed from the set of landmarks $\boldsymbol{x_L}$ to keep the segmented contour consistent with the image features. Although, in practice, it is better to use a few more landmark points to avoid this problem. It is worth noting that in [31], the landmarks initially detected are clusters rather than points. Methods that detect a larger number of landmark points can be used to our advantage in CVL.

6. Conclusions

In this paper, we proposed a modified Chan-Vese model incorporating landmark information featured as constraints. Then, we designed the numerical solution of the new model with the Split Bregman method with projection. Finally, we investigated the mathematical properties of the solution to the CVL and analyzed the theoretical performance of the model.

Experiments show that the CVL model can effectively use landmark information to improve segmentation results as well as lower the dependence on the initial contour and other parameter settings, which raises the practicality and general performance of the Chan-Vese model. In the case of segmenting objects with more complicated interiors, the Chan-Vese model still has many limitations, especially compared to contour-based models [6,7]. Additionally, the two-phase model is not enough to describe real-life scenarios, but rather serves as a basis for multi-phase models. In future works, the landmark constraints can be implemented in multi-phase models as well as contour-based models to address more problems in image segmentation. Moreover, the CVL can be combined with deep learning modules for detecting landmarks such as [31] to automate the segmentation process further.

References

[1] D. Cremers, M. Rousson, R. Deriche, A review of statistical approaches to level set segmentation: integrating color, texture, motion and shape, Int. J. Comput. Vision 72 (2) (2007) 195–215 doi:10.1007/s11263-006-8711-1.
[2] G. Aubert, P. Kornprobst, Mathematical Problems in Image Processing: Partial Differential Equations and the Calculus of Variations, Springer, 2006.
[3] T.F. Chan, J.J. Shen, Image Processing and Analysis: Variational, PDE, Wavelet, And Stochastic Methods, Siam, 2005.
[4] L.A. Vese, C. Le Guyader, Variational Methods in Image Processing, CRC Press, 2015.
[5] A. Mitiche, I.B. Ayed, Variational and Level Set Methods in Image Segmentation, Vol. 5, Springer, 2010.
[6] M. Kass, A. Witkin, D. Terzopoulos, Snakes: Active contour models, Int. J. Comput. Vision 1 (4) (1988) 321–331.
[7] V. Caselles, R. Kimmel, G. Sapiro, Geodesic active contours, Int. J. Comput. Vision 22 (1) (1997) 61–79.
[8] D. Mumford, J. Shah, Optimal approximations by piecewise smooth functions and associated variational problems, Commun. Pure Appl. Math. 42 (5) (1989) 577–685.
[9] S. Solimini, J. Morel, Variational methods in image segmentation, Progress in Nonlinear Differential Equations and Their Applications.
[10] T.F. Chan, L.A. Vese, Active contours without edges, IEEE Trans. Image Process. 10 (2) (2001) 266–277, https://doi.org/10.1109/83.902291.
[11] S. Osher, J.A. Sethian, Fronts propagating with curvature-dependent speed: algorithms based on hamilton-jacobi formulations, J. Comput. Phys. 79 (1) (1988) 12–49.
[12] H.-K. Zhao, T. Chan, B. Merriman, S. Osher, A variational level set approach to multiphase motion, J. Comput. Phys. 127 (1) (1996) 179–195.
[13] T.F. Chan, B.Y. Sandberg, L.A. Vese, Active contours without edges for vector-valued images, J. Visual Commun. Image Represent. 11 (2) (2000) 130–141.
[14] C. Sagiv, N.A. Sochen, Y.Y. Zeevi, Integrated active contours for texture segmentation, IEEE Trans. Image Process. 15 (6) (2006) 1633–1646.
[15] C. Samson, L. Blanc-Féraud, G. Aubert, J. Zerubia, A variational model for image classification and restoration, IEEE Trans. Pattern Anal. Mach. Intell. 22 (5) (2000) 460–472.
[16] L.A. Vese, T.F. Chan, A multiphase level set framework for image segmentation using the mumford and shah model, Int. J. Comput. Vision 50 (3) (2002) 271–293.
[17] D. Cremers, S. Soatto, Motion competition: a variational approach to piecewise parametric motion segmentation, Int. J. Comput. Vision 62 (3) (2005) 249–265.
[18] W. Zhu, X.-C. Tai, T. Chan, Image segmentation using Euler's Elastica as the regularization, J. Sci. Comput. 57 (2) (2013) 414–438.
[19] C. Li, C. Xu, C. Gui, M.D. Fox, Level set evolution without re-initialization: a new variational formulation, in: Computer Vision and Pattern Recognition, 2005. CVPR 2005, IEEE Computer Society Conference on, Vol. 1, IEEE, 2005, pp. 430–436.
[20] J. Duan, Z. Pan, X. Yin, W. Wei, G. Wang, Some fast projection methods based on chan-vese model for image segmentation, EURASIP J. Image Video Process. 2014 (1) (2014) 7.
[21] K. Rohr, Landmark-based image analysis: using geometric and intensity models, Vol. 21, Springer, 2001.
[22] J. Modersitzki, Numerical Methods for Image Registration, Oxford University Press, 2004.
[23] S. Banik, R.M. Rangayyan, G.S. Boag, Landmarking and segmentation of 3d ct images, Synthesis Lect. Biomed. Eng. 4 (1) (2009) 1–170.
[24] W.-H. Liao, A. Khuu, M. Bergsneider, L. Vese, S.-C. Huang, S. Osher, From landmark matching to shape and open curve matching: a level set approach, UCLA CAM Report 2 (59).
[25] D. Seghers, P. Slagmolen, Y. Lambelin, J. Hermans, D. Loeckx, F. Maes, P. Suetens, Landmark based liver segmentation using local shape and local intensity models, in: Proc. Workshop of the 10th Int. Conf. on MICCAI, Workshop on 3D Segmentation in the Clinic: A Grand Challenge, 2007, pp. 135–142.
[26] T. Lin, E.-F. Lee, I. Dinov, C. Le Guyader, P. Thompson, A.W. Toga, L.A. Vese, A landmark-based nonlinear elasticity model for mouse atlas registration, in: Biomedical Imaging: From Nano to Macro, 2008. ISBI 2008. 5th IEEE International Symposium on, IEEE, 2008, pp. 788–791.
[27] B. Fischer, J. Modersitzki, Combination of automatic non-rigid and landmark based registration: the best of both worlds, in: Medical Imaging 2003: Image Processing, Vol. 5032, International Society for Optics and Photonics, 2003, pp. 1037–1049.
[28] A. Ghaffari, R. Khorsandi, E. Fatemizadeh, Landmark and intensity based image registration using free form deformation, in: Biomedical Engineering and Sciences (IECBES), 2012 IEEE EMBS Conference on, IEEE, 2012, pp. 768–771.
[29] K.C. Lam, L.M. Lui, Landmark-and intensity-based registration with large deformations via quasi-conformal maps, SIAM J. Imaging Sci. 7 (4) (2014) 2364–2392.
[30] F. Brunet, V. Gay-Bellile, A. Bartoli, N. Navab, R. Malgouyres, Feature-driven direct non-rigid image registration, Int. J. Comput. Vision 93 (1) (2011) 33–52.
[31] J. Duan, G. Bello, J. Schlemper, W. Bai, T. J. Dawes, C. Biffi, A. de Marvao, G. Doumou, D. P. O'Regan, D. Rueckert, Automatic 3d bi-ventricular segmentation of cardiac images by a shape-constrained multi-task deep learning approach, arXiv preprint arXiv:1808.08578.

[32] Y. Ren, Q. Li, W. Liu, L. Li, Semantic facial descriptor extraction via axiomatic fuzzy set, Neurocomputing 171 (2016) 1462–1474.
[33] D. Li, Y. Ren, T. Du, W. Liu, Eyebrow semantic description via clustering based on axiomatic fuzzy set, Wiley Interdisciplinary Reviews: Data Mining and Knowledge Discovery 8 (6) (2018) e1275.
[34] C. Wu, X.-C. Tai, Augmented Lagrangian method, dual methods, and Split Bregman iteration for ROF, vectorial TV, and high order models, SIAM J. Imaging Sci. 3 (3) (2010) 300–339.
[35] T. Goldstein, S. Osher, The Split Bregman method for l1-regularized problems, SIAM J. Imaging Sci. 2 (2) (2009) 323–343.
[36] L. Tan, Z. Pan, W. Liu, J. Duan, W. Wei, G. Wang, Image segmentation with depth information via simplified variational level set formulation, J. Math. Imaging Vision 60 (1) (2018) 1–17.
[37] T. Goldstein, B. O'Donoghue, S. Setzer, R. Baraniuk, Fast alternating direction optimization methods, SIAM J. Imaging Sci. 7 (3) (2014) 1588–1623.
[38] H. Huang, X. Zuo, C. Huang, Arbitrary initialization for chan-vese model, Optik 125 (18) (2014) 5257–5263.
[39] J. Nocedal, S.J. Wright, Nonlinear Equations, Springer, 2006.